Journal of Atmospheric and Solar-Terrestrial Physics 184 (2019) 30–36

Contents lists available at ScienceDirect

Journal of Atmospheric and Solar-Terrestrial Physics

journal homepage: www.elsevier.com/locate/jastp

# Distinct thermospheric mass density variations following the September 2017 geomagnetic storm from GRACE and Swarm

Liangliang Yuan[a,b], Shuanggen Jin[a,c,*], Andres Calabia[c]

[a] Shanghai Astronomical Observatory, Chinese Academy of Sciences, Shanghai, 200030, China
[b] University of Chinese Academy of Sciences, Beijing, 100049, China
[c] School of Remote Sensing and Geomatics Engineering, Nanjing University of Information Science and Technology, Nanjing, 210044, China

ARTICLE INFO

*Keywords:*
Thermospheric density
POD
Geomagnetic storm
Swarm
GRACE

ABSTRACT

Geomorphologies and mechanisms of thermospheric mass density variations caused by geomagnetic storms are still challenging due to limited observations and imprecise models. Recently, precise orbit determination (POD) of Gravity Recovery and Climate Experiment (GRACE) and Swarm satellites is able to estimate thermospheric mass density variations, which may provide data to study thermospheric mass density variations following the storm. In this paper, the thermospheric mass density is estimated from GRACE-A and Swarm-A POD and the distinct thermospheric mass density variations are investigated as function of latitude during the September 2017 geomagnetic storm. Different enhancements in mass density response to the geomagnetic storm are presented for the Northern (GRACE) and the Southern (Swarm) Hemispheres. Swarm observations show symmetric mass density variations between two hemispheres and a slightly stronger enhancement in Southern Hemisphere. GRACE POD and accelerometer observations both show a very strong enhancement in Northern Hemisphere while no corresponding enhancement in Southern Hemisphere. This anomaly may attribute to the effects of vertical winds in high latitude region and plasma drift considering the similar solar zenith angles in both hemispheres.

## 1. Introduction

Main dynamic disturbances at Low Earth Orbit (LEO) satellites are caused by changes of thermospheric mass density due to atmospheric expansions caused by variations of solar activity. Therefore, the exact modeling of thermospheric mass density variations is a very important in Precise Orbit Determination (POD) of debris, unmanned objects, and active satellites as well as precise applications [Jin et al., 2018; Jin and Zhu, 2001]. In the thermosphere, the coupling between ion and neutral particles is mainly driven by the solar activity and Earth's magnetic field, where the neutral density is very low and the dynamics are rather driven by the Extreme Ultra Violet (EUV) heating instead by the intermolecular interactions [Forbes and Roble, 1990; Jin et al., 2013]. In addition, rapid abrupt changes of thermospheric density and composition occur during geomagnetic storms [Forbes et al., 1996], and the involved geophysical processes are still not well understood or modeled as required for POD.

In the recent decades, accelerometer and POD have been the two major approaches to derive thermospheric total mass density estimates [Bruinsma et al., 2004; McLaughlin et al., 2013; Calabia and Jin, 2017], and widely employed to investigate thermospheric variations driven by Joule heating and air upwelling during geomagnetic storms [Forbes et al. (1996); Bruinsma et al. (2006); Calabia and Jin (2016a and 2016b). Thermospheric mass density responses to geomagnetic storms are more apparent in the high-latitude regions, near the cusp, where the solar wind can access easily into the upper atmosphere through the Earth's magnetic reconnection. Furthermore, in situ abrupt heating in the cusp can produce equatorward gravity waves [Bruinsma et al., 2006].

During a magnetic storm, the energy in the thermosphere can be transferred from high to low latitudes through both gravity waves and meridional circulation [Richmond, 1979]. Moreover, disturbances in the high-latitude region propagate equator-ward through atmosphere circulation, reaching in few hours in the middle and lower latitudes. Calabia et al., [2017] have recently provided the correlation index and time-delay for the most representative geomagnetic indices, as well as the time to reach the equatorial region. Studying the thermospheric density variability during geomagnetic storms is of high importance for Magnetosphere-Ionosphere-Thermosphere (MIT) coupling research and POD applications and for the improvement of current models used in

* Corresponding author. Shanghai Astronomical Observatory, Chinese Academy of Sciences, Shanghai, 200030, China.
*E-mail addresses:* sgjin@shao.ac.cn, sg.jin@yahoo.com (S. Jin).

https://doi.org/10.1016/j.jastp.2019.01.007
Received 9 October 2018; Received in revised form 9 January 2019; Accepted 10 January 2019
Available online 11 January 2019
1364-6826/ 

POD. For instance, previous researches (e.g., Calabia and Jin [2016b], Calabia and Jin [2017], Calabia and Jin [2016b], Calabia and Jin [2017]) have proven that the latest empirical model NRLMSISE00 [Picone et al., 2002], standard used for POD, is currently unable to accurately reproduce and predict the mean value and LST amplitude of variability of the actual thermospheric density states during geomagnetic storms.

Burns et al., [2004] inferred that density variability depends on the background quiet-time state and vary from season to season. Their simulation results showed that the density variability in winter is higher than that in the summer under the same magnetospheric inputs. This feature is attributed to differences in solar heating. Moreover, based on Challenging Minisatellite Payload (CHAMP) accelerometer-based estimates, the results in Liu and Lühr [2005] showed small differences between the day-side and the night-side relative percentage changes, and that the response of thermospheric density during storm time is not similar from event to event. The westward equatorial flow following the diurnal variation of EUV heating is especially obvious in the night side, but it is difficult to investigate due to the large intervals between CHAMP recurrence sampling, and the convection driven by meridional and zonal winds is not sensitive to those observations [Sutton et al., 2005]. Sutton et al., [2005] showed density enhancements of about 300–800% during the geomagnetic storm in November 2003. The time-delay with respect to proxies showed shorter at high latitudes than at lower latitudes, being the later about 4-hour. Day side densities at 410 Km altitude in the high-latitude Southern hemisphere in Summer (i.e., $-72^{\circ}$ geomagnetic latitude) at noon LST are very responsive to increases in solar wind dynamic pressure, and even during periods when both Bz and By are near zero or positive [Bruinsma et al., 2006].

This paper focuses on the detailed responses of thermospheric POD-based mass density during the geomagnetic storm of September 2017 from GRACE and Swarm satellites. Section 2 describes the data and methods employed in this study. Section 3 presents the detailed results and the relational aspects with space weather indices and comparison between GRACE POD and Accelerometer observations as well as discussions in Section 4. Finally, some conclusions are given in Section 5.

## 2. Data and methods

### 2.1. Geomagnetic indices

Fig. 1 shows the time series of Space Weather measurements, including the interplanetary magnetic field (IMF) Bx, By, Bz, the Field Magnitude Average (FMA), the Plasma Speed (PS), and the Electric Field (EF), which have been downloaded from https://spdf.gsfc.nasa.gov/. The first geomagnetic storm started with a Storm Sudden Commencement (SSC) [Araki, 1994] started at 1100 UT on 7 September 2017. The main phase (MP) starts at 2307 UT on 7 September and reaches its maximum phase (SYM-H = −146 nT) at around 0108 UT on 8 September. And the latter storm reached its maximum phase (SYM-H = −115 nT) at around 1356 UT on 8 September. IMF Bz remains strongly southward during the main phase (2100UT-0100UT and 1200UT-1400UT on 8 Sep). The minimum Bz value of IMF was −23.6 nT and −13.9 nT in the main phase of the two geomagnetic storms.

### 2.2. Thermospheric mass density retrieval

In this work, POD-based thermospheric mass density estimates are derived from the Level 1B data of GRACE-A and Swarm-A missions, including accelerometer, navigation, thruster, and star-camera measurements, among others. GRACE's Level 1B data can be downloaded from http://isdc-old.gfz-potsdam.de in binary big-endian format, and Swarm's Level 1B data can be downloaded from ftp://Swarm-diss.eo.esa.int in CDF (Common Data Format). More details and metadata can be found in the respective links.

We employ the method developed in Calabia et al., [2015] and Calabia and Jin [2017] for accelerometer calibration and POD-based thermospheric mass density retrieval. The method is based on the de-gravitation of numerically differentiated precise orbit velocities, where a first step employs the arc-to-chord method in a piecewise interpolation scheme to minimize the arc-to-chord error committed in the numerical differentiation. In this scheme, POD-based total accelerations are derived from Precise Orbit velocities as follows:

$$\ddot{r}_{t0} = \lim_{Dt \to 0} \frac{r_{t2} - 2r_{t0} + r_{t(-2)}}{(Dt)^2}, \quad where\ t\left(i+1\right) - t(i) = Dt \tag{1}$$

The following step is to de-gravitate or, in other words, remove from

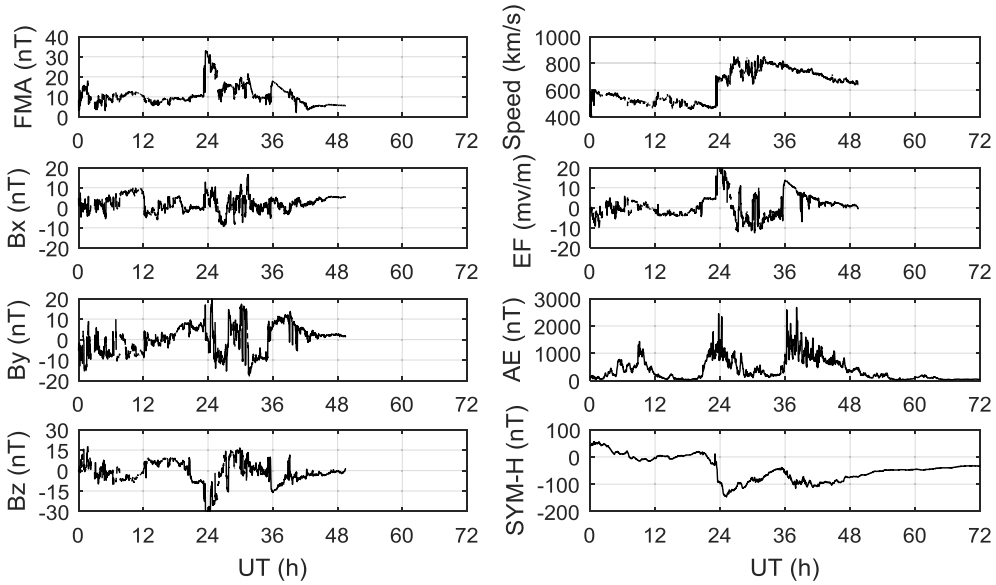


**Fig. 1.** Space weather indices during the 7–9 September 2017 geomagnetic storm events. The storm sudden commencements (SSCs) occurred at 2302 h UT on 7 September 2017.

POD-based total accelerations the effects of the time-varying gravity. The time-varying gravity at the satellite location is accurately estimated through models, where the static average gravitational field is combined with the variable contributions, including the trends of the low-degree Stokes coefficients, solid tides, permanent tides, ocean tides, polar tides and others. The standard form to compute the variable Earth's gravitational potential is given by:

$$V\left(r, j, l\right) = \frac{GM_{Earth}}{r}\sum_{n=0}^{N}\left(\frac{a_e}{r}\right)^n\sum_{m==0}^{n}[\overline{C_{nm}}cos\left(ml\right) + \overline{S_{nm}}sin\left(ml\right)]\overline{P_{nm}}sin\left(j\right) \quad (2)$$

where $G$ is the gravitational constant, $M_{\text{Earth}}$is the mass of the Earth, $r$the distance to the mass center of the Earth, $a_e$ the semi-major axis of the Earth. $GM_{\text{Earth}}$ and $a_e$ values in EGM2008 (398600.4415 $km^3/s^2$ and 6378136.3m respectively) should be used as scaling parameters with its gravitational potential coefficients.

The gravity model is calculated at the ITRS (International Terrestrial Reference System), but the non-gravitational accelerations are given at the SBS (Satellite Body System). Therefore, the time-variable gravity in the ITRS has to be transformed to the ICRS (International Celestial Reference System) through the star camera quaternion measurements. Moreover, the residual accelerations in the ICRF have to be transformed to the SBS (Satellite Body System) to remove the three-body perturbation and the relativistic effects. Non-gravitational accelerations are finally given in the SBS frame to be compared with accelerometer measurements if available.

In order to derive the pure aerodynamic accelerations, direct solar radiation pressure (direct and reflected) and Earth's albedo radiation need to be removed from the non-gravitational accelerations obtained in the previous step. The final step is to obtain the air mass density along the orbital path through the aerodynamic drag equation

$$F_D = \frac{1}{2}CA\rho v_r^2 \quad (3)$$

$$\mathrm{v_r} = -\dot{r}_{sat} + v_c + v_w \quad (4)$$

In this study, we set the drag coefficient $C$ to the ESA recommended value of 2.2. $A$ is the cross-sectional area perpendicular to $v_r$ , $\rho$ is the mass density, and $v_r$ is the relative velocity of the atmosphere with respect to the spacecraft, which includes the co-rotating atmosphere $v_c$ and horizontal winds $v_w$.

## 3. Results and analyses

### 3.1. POD-based non-gravitational accelerations

GRACE's POD-based non-gravitational accelerations are first contrasted to accelerometer measurements. We employ the POD solution to calibrate accelerometer measurements. Fig. 2 shows the comparison of our POD-based with the calibrated-accelerometer non-gravitational accelerations from GRACE-A on 8 September 2017.

On the other side, in Fig. 3 we compare Swarm's POD-based non-gravitational accelerations computed through our numerical derivation with the ESA's POD-based non-gravitational accelerations derived using a Kalman Filter on a least-squares POD scheme with the reduced-dynamic solution as a reference. The low performance of Swarm-A accelerometers forced us to compare our results with Swarm-A ESA POD product. From Fig. 3, we can see that the non-gravitational accelerations along track are in a good consistence with ESA product.

### 3.2. Thermospheric density variations

The algorithm to derive mass density along the orbital path of GRACE and Swarm (Equation (3)) has been used to estimate mass density from the POD-based non-gravitational accelerations during the September 8th, 2017 geomagnetic storm. We employ the surrounding quiet period, past three days in this study, to evaluate percentage changes during the storm. But accelerometer measurements of GRACE were not available during the adjacent periods. The accelerometer measurements of Swarm-A during this storm are also not available. However, POD-based non-gravitational accelerations provide us the opportunity to derive and investigate mass density variations. Fig. 4 shows the mass density retrieved form POD, accelerometer, and from the NRLMSISE00 model. Clear differences are seen between the model and measurements, indicating the lack of detail from the model to reproduce mass density variations during the storm.

As it can be seen from the change in the IMF parameters in Fig. 1, the peak of the two geomagnetic storms is located at 0 h UT and at 12 h UT on the 8th, respectively. Swarm and GRACE missions have a quasi-polar orbit and their latitudes range from 88° S to 88° N, while Swarm's Local Solar Time (LST) is located at about 10:00 h LST at the ascending orbit and 22:00 h LST at the descending orbit, and therefore divide our analysis into these two parts. GRACE's LST at this period is located at about 21:30 h LST at the ascending orbit and about 9:30 h LST at the descending orbit, so this is an ideal configuration since Swarm has a similar LST location.

Figs. 5 and 7 show the mass density variability along the orbital path of GRACE and Swarm, respectively. Figs. 6 and 8 present the same figures with normalized values at altitudes of 350 Km and 450 Km, respectively. The averaged atmospheric density at the day-side (10 h LST) shows higher values than the values at the night-side (22 h LST). It can be seen that two density peaks are located at around 0h and 12 h UT during the geomagnetic storm, the average atmospheric density on the day side is significantly higher than that on the night side for both missions, and the short-term variations well correlated with the geomagnetic indices.

### 3.3. Density variability with latitude

During the initial phase of the geomagnetic storm, the GRACE-A results shown in Fig. 6 reveal a stronger response in the Northern hemisphere than in the Southern hemisphere. The global atmospheric density does not show an increase at this stage. On the other side, Swarm shows a slightly stronger response in the Southern hemisphere. It is interesting to note that at Equinox periods density values are

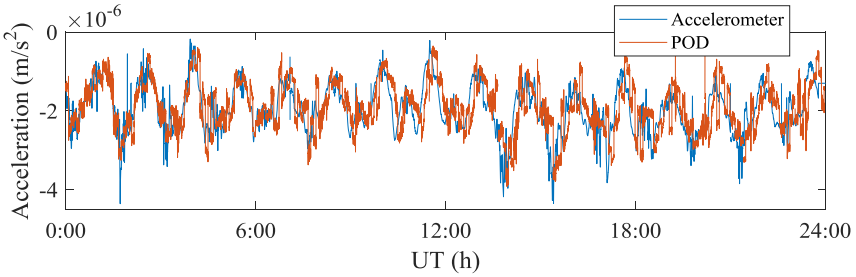


**Fig. 2.** The comparison of our POD-based and calibrated-accelerometer non-gravitational accelerations from GRACE-A on September 8th, 2017.

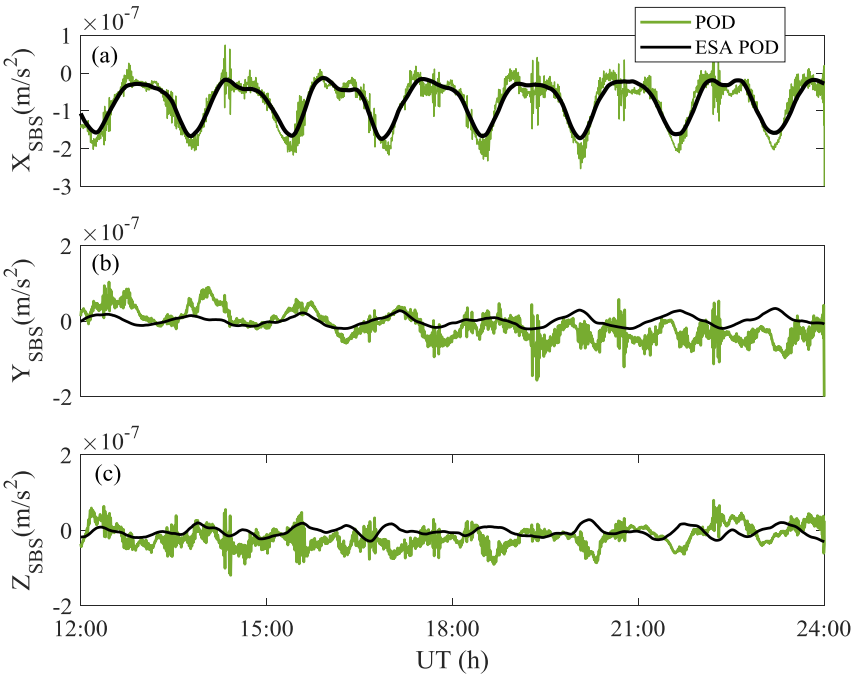


**Fig. 3.** The comparison of POD-based non-gravitational accelerations from our results and from the official ESA products for Swarm-A on September 7th, 2017.

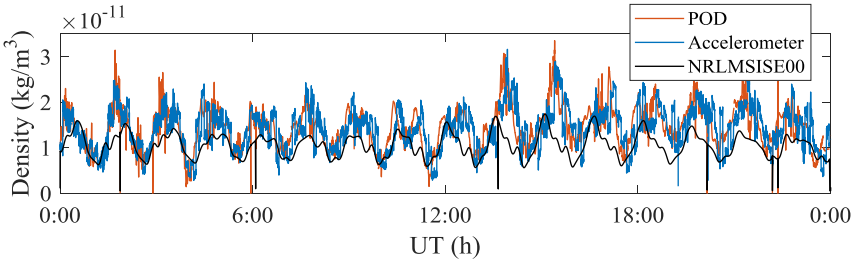


**Fig. 4.** The comparison of accelerometer-based thermospheric mass density from GRACE-A, our POD-based results, and the NRLMSISE00 estimates on September 8th, 2017.

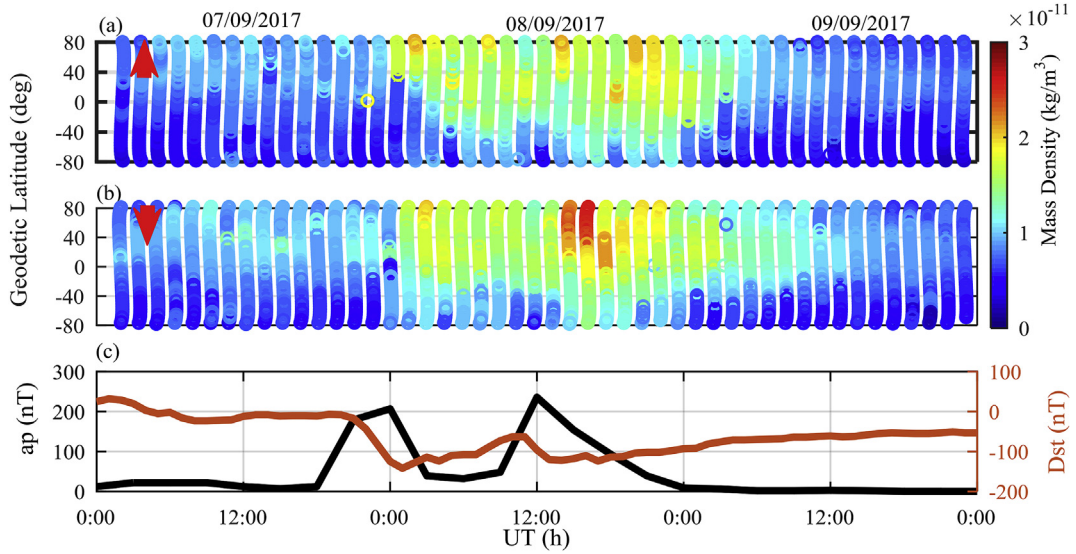


**Fig. 5.** POD-based thermospheric density variability from (a) ascending (21:30 h LST) and (b) descending orbits (9:30 h LST), from GRACE-A at orbital altitude during the geomagnetic storm on September 8th, 2017.

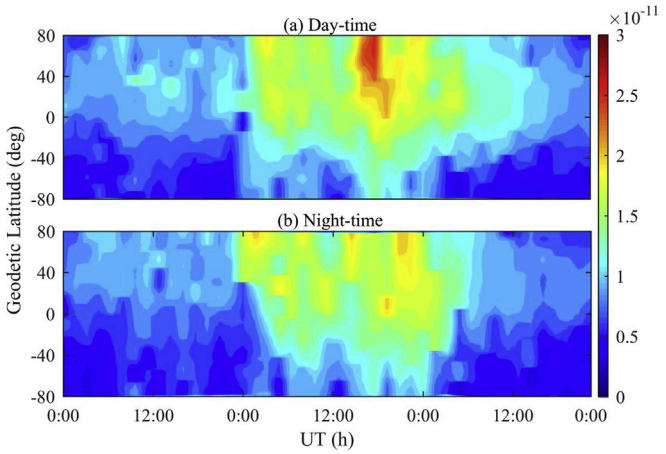


**Fig. 6.** Panels from Fig. 5 normalized at 350 Km altitude. Top panel (a) for day-time and bottom panel (b) for night-time.

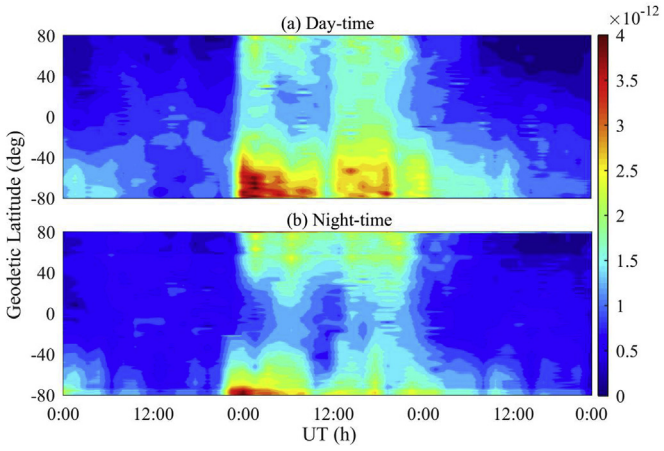


**Fig. 8.** Panels from Fig. 7 normalized at 450 Km altitude. Top panel (a) for day-time, and bottom panel (b) for night-time.

enhanced at the Southern latitude, suggesting a higher cusp precipitation probably related to the dipole-tilt angle variation [Calabia et al, 2017]. Moreover, from Fig. 6 it seems that this effect is less pronounced at a lower altitude.

During the main phase of the second geomagnetic storm, the global thermospheric density of Swarm rapidly increases. Fig. 8 shows that the Southern hemisphere density values observed by Swarm are bigger than those for the Northern hemisphere. This enhancement increases and rapidly covers more latitudinal ranges, especially in the daytime. On the other side for GRACE, Fig. 6 shows a strong asymmetry of thermospheric density enhancement.

Initially, density enhancements during geomagnetic storms occur in the Polar Regions. Afterwards, the enhancements will propagate to lower latitudes due to density gradients, meridional winds, and gravity wave. Fig. 9 shows a cross-correlation analysis of density disturbance observed by Swarm in Polar regions (60°–90°) and equatorial regions (−15°-15°). As it can be seen in Figs. 8 and 9 from the two major turning points at which the slope of correlation line changes suddenly, the propagation toward lower latitudes is faster at the day side than at the night side. During night time, there is an apparent time lag between southern hemisphere and equatorial region, but there is no apparent asymmetry between the time lags of both hemispheres at the day side, which probably relates to the similar solar radiation on both hemispheres in September Equinox.

The main difference lies in that for GRACE observation, the strength of second storm is stronger than the first one. This is clearly seen with the higher maximum values of density for the second storm, and especially at high latitudes. Fig. 6 shows a strong asymmetry of density enhancement between Northern and Southern Hemisphere, which is compared with accelerometer observations and discussed in next section.

## 4. Discussion

Due to the fact that there are some disturbances and outliers in GRACE POD result, it is necessary to validate the POD results with accelerometer observations. Fig. 10 illustrates the thermospheric density based on calibrated accelerometer observations, which shows that accelerometer observations are generally consistent with POD results. Both POD results and accelerometer observations show a similar strong hemisphere asymmetry which indicates that these two storms lead to a strong enhancement of the thermospheric density at 350 Km in Northern high latitude region at first and then the density enhancement propagates to equatorial region while there is a very weak density

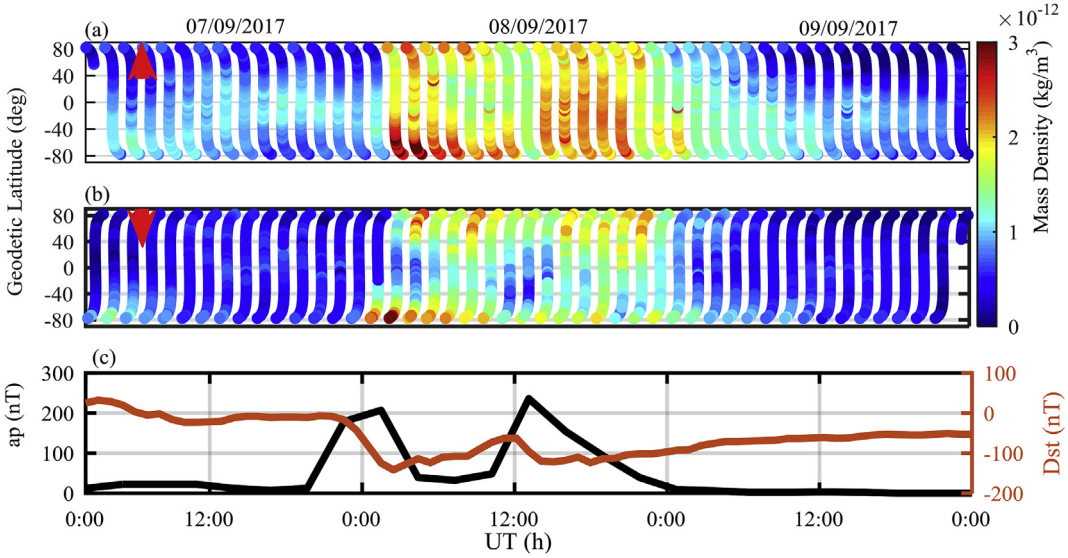


**Fig. 7.** POD-based thermospheric density variability from (a) ascending (10:00 h LST) and (b) descending orbits (22:00 h LST), from Swarm-A at orbital altitude during the geomagnetic storm of September 8th, 2017.

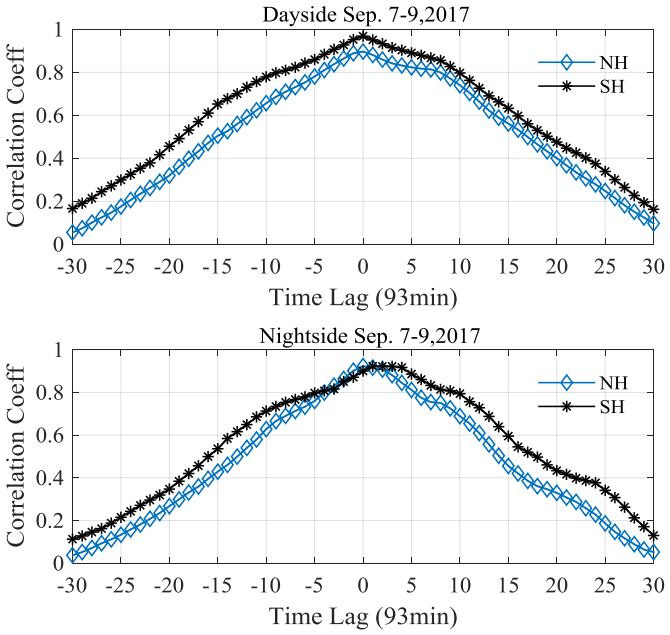


**Fig. 9.** Cross-correlation analysis of density disturbance observed by Swarm in polar regions (60°–90°) and equatorial regions (−15°-15°). Positive time lag means that equatorial region density disturbance is later than polar region density disturbance.

enhancement in Southern high latitude region. When comparing Figs. 8 and 10, there are two completely contrary hemisphere asymmetric features at 350 km and 450 km. Besides, the thermospheric density at 350 km is more sensitive to the first storm than the second storm while that at 450 km is more sensitive to the second storm. It can be concluded that these two geomagnetic storms effects on thermospheric density are entirely different at the height of GRACE and Swarm. In interpreting these hemispheric differences in the responses at high latitudes, it must be remembered that conditions are within 20 days of September Equinox. And therefore both hemispheres are subject to similar solar zenith angles, and hence similar electrical conductivities. Referring to Fig. 1 that shows in most of storm time Bz remains negative. It can be expected that in Southern Hemisphere there is a slightly stronger density enhancement as Swarm POD results show. However, Neither GRACE POD nor accelerometer observations detect such an expected feature. Considering the lower thermosphere and ionosphere coupling, the anomaly along GRACE orbit may attribute to the effects of vertical winds in high latitude region and plasma drift [Crowley et al., 2008]. It can also be expected in Fig. 10 that during day-time the propagation of thermospheric density enhancement is slower than during night-time because of the EUV-driven poleward wind that inhibits the equatorward propagation [Bruinsma et al., 2006]. Meanwhile, during day-time the density enhancement can easily cross the equatorial region thanks to the dominant thermal expansion at low latitude region while during night-time the density enhancement can only reach the equatorial region without further propagation in Southern Hemisphere.

For Swarm observations, the density enhancements at high latitude during the first geomagnetic storm are stronger than those during the second storm, which is also expectable from the weaker IMF disturbances such as Bz and SYM-H during second storm. But for GRACE observations, the case is also contrary with Swarm, which indicate that the enhancements of mass density at GRACE orbit are probably dominated by the coupling between ionosphere and thermosphere instead of the geomagnetic conditions.

## 5. Conclusion

This work has investigated the thermospheric mass density variability in latitude during the September 2017 geomagnetic storms as seen from Swarm and GRACE observations. Different enhancements in mass density response to the geomagnetic storm are presented for the Northern (GRACE) and the Southern (Swarm) Hemispheres. Main results and conclusions are as following:

1. Swarm observations show symmetric mass density variations between two hemispheres and a slightly stronger enhancement in Southern Hemisphere, which are expectable according to the IMF conditions and the solar radiation.
2. At the night side there is a roughly 93min time lag in density enhancement between southern hemisphere and equatorial region from Swarm observations, but there is no such asymmetry between the time lags of density enhancement at the day side.
3. GRACE POD and accelerometer observations both show a very strong enhancement in Northern Hemisphere while no corresponding enhancement in Southern Hemisphere. This anomaly may attribute to the effects of vertical winds in high latitude region and

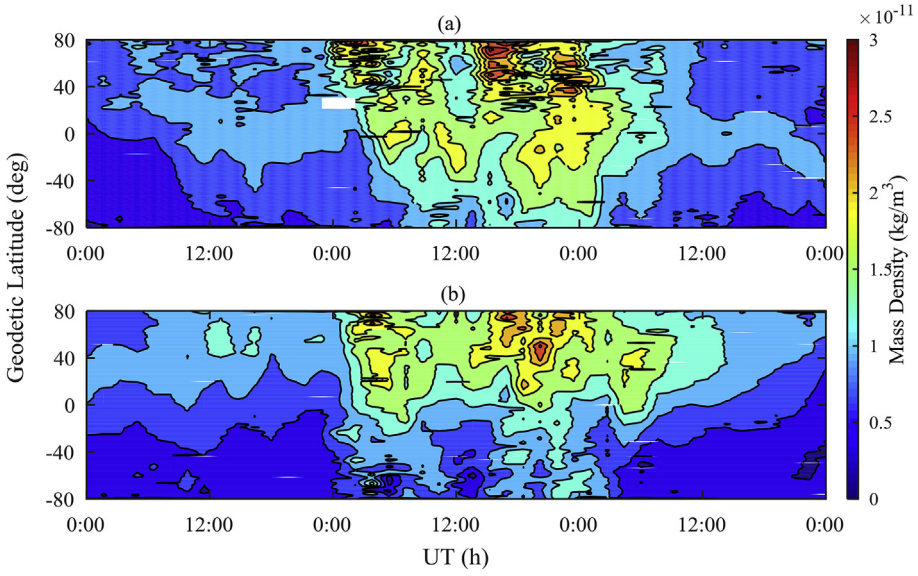


**Fig. 10.** Thermospheric density at 350 Km from GRACE accelerometer observations. Top panel (a) for day-time and bottom panel (b) for night-time.

plasma drift considering the similar solar zenith angles in both hemispheres within 20 days of September Equinox and similar local time of these two satellites.
4. During day-time the propagation of thermospheric density enhancement at GRACE orbit is slower than during night-time because of the EUV-driven poleward wind that inhibits the equatorward propagation. Meanwhile, during day-time the density enhancement can easily cross the equatorial region due to the dominant thermal expansion at low latitude region.
5. The thermospheric behavior at 350 km is probably dominated by the coupling between ionosphere and thermosphere instead of the geomagnetic conditions, which need to be further verified with possible observations or simulations.

The thermospheric density variability at different altitudes is important for studying the coupling mechanisms and for the calibration of upper atmospheric models. Further studies are needed in the future for a better modeling of mass density disturbances during high geomagnetic activity.

## Author's contributions

LY and SJ planned the whole research. LY conducted data analysis and wrote the manuscript. AC helped to provide guidance and scripts for density retrieval. All members read the manuscript and agreed on the content.

## Conflicts of interest

The authors have no competing interest.

## Availability of data and materials

All the data used in this manuscript can be provided on request.

## Funding

This study was supported by the National Natural Science Foundation of China (NSFC) Project Grant Numbers 11573052 and 41761134092.

## Acknowledgments

We thank the Information System and Data Center (ISDC) GeoForschungsZentrum (GFZ) (http://isdc.gfz-potsdam.de) for providing the GRACE data. We also thank the European Space Agency (ESA) (https://earth.esa.int/web/guest/swarm/data-access) for providing the Swarm data.

## Appendix A. Supplementary data

Supplementary data to this article can be found online at https://doi.org/10.1016/j.jastp.2019.01.007.

## References

Araki, T., 1994. A physical model of the geomagnetic sudden commencement. In: In: Engebretson, M., Takahashi, K., Scholer, M. (Eds.), Solar Wind Sources of Magnetospheric Ultra-low Frequency Waves, Geophys. Monogr. Ser, vol. 81. AGU, Washington, D. C. USA, pp. 183–200.

Bruinsma, S., Tamagnan, D., Biancale, R., 2004. Atmospheric densities derived from CHAMP/STAR accelerometer observations. Planet. Space Sci. 52, 297–312. https://doi.org/10.1016/j.pss. 2003.11.004.

Bruinsma, S., Forbes, J.M., Nerem, R.S., Zhang, X., 2006. Thermosphere density response to the 20–21 November 2003 solar and geomagnetic storm from CHAMP and GRACE accelerometer data. J. Geophys. Res. 111, A06303. https://doi.org/10.1029/2005JA011284.

Burns, A.G., Killeen, T.L., Wang, W., Roble, R.G., 2004. The solar cycle dependent response of the thermosphere to geomagnetic storms. J. Atmos. Terr. Phys. 66, 1–14.

Calabia, A., Jin, S.G., Tenzer, R., 2015. A new GPS-based calibration of GRACE accelerometers using the arc-to-chord threshold uncovered sinusoidal disturbing signal. Aero. Sci. Technol. https://doi.org/10.1016/j.ast.2015.05.013.

Calabia, A., Jin, S.G., 2016a. Thermospheric mass density variations during the March 2015 geomagnetic storm from GRACE accelerometers. In: Proceeding of Progress in Electromagnetics Research Symposium (PIERS2016), August 8-11, 2016, Shanghai, China, pp. 4976–4980. https://doi.org/10.1109/PIERS.2016.7735812.

Calabia, A., Jin, S.G., 2016b. New modes and mechanisms of thermospheric mass density variations from GRACE accelerometers. J. Geophys. Res. Space Phys. 121 (11), 11191–11212. https://doi.org/10.1002/2016JA022594.

Calabia, A., Jin, S.G., 2017. Thermospheric density estimation and responses to the March 2013 geomagnetic storm from GRACE GPS-determined precise orbits. J. Atmos. Sol. Terr. Phys. 154, 167–179. https://doi.org/10.1016/j.jastp.2016.12.011.

Calabia, A., Jin, S.G., Matsuo, T., 2017. Modeling of thermospheric neutral density variations in response to geomagnetic forcing using GRACE accelerometer data. In: Abstract SA22A-04 Presented at 2017 Fall Meeting. AGU, New Orleans, LA 11-15 Dec.

Crowley, G., Reynolds, A., Thayer, J.P., Lei, J., Paxton, L.J., Christensen, A.B., Zhang, Y., Meier, R.R., Strickland, D.J., 2008. Periodic modulations in thermospheric composition by solar wind high speed streams. Geophys. Res. Lett. 35, L21106. https://doi.org/10.1029/2008GL035745.

Forbes, J.M., Roble, R.G., 1990. Thermosphere-ionosphere coupling: an experiment in interactive modeling. J. Geophys. Res. 95 (A1), 201–208. https://doi.org/10.1029/JA095iA01p00201.

Forbes, J.M., Gonzalez, R., Marcos, F.A., Revelle, D., Parish, H., 1996. Magnetic storm response of lower thermospheric density. J. Geophys. Res. 101, 2313–2319.

Jin, S.G., Calabia, A., Yuan, L.L., 2018. Thermospheric variations from GNSS and accelerometer measurements on small satellites. Proc. IEEE 106 (3), 484–495. https://doi.org/10.1109/JPROC.2018.2796084.

Jin, S.G., Arivazhagan, S., Araki, H., 2013. New results and questions of lunar exploration from SELENE, Chang'E-1, Chandrayaan-1 and LRO/LCROSS. Adv. Space Res. 52 (2), 285–305. https://doi.org/10.1016/j.asr.2012.11.022.

Jin, S.G., Zhu, W.Y., 2001. Analysis of improving the precision of InSAR with GPS measurements. J. Rem. Sens. Info. 4, 8–11.

Liu, H., Lühr, H., 2005. Strong disturbance of the upper thermospheric density due to magnetic storms: CHAMP observations. J. Geophys. Res. 110, A09S29. https://doi.org/10.1029/2004JA010908.

McLaughlin, C.A., Lechtenberg, T., Fattig, E., Mysore Krishna, D., 2013. Estimating density using precision satellite orbits from multiple satellites. J. Astronaut. Sci. 59 (1–2), 84–100. https://doi.org/10.1007/s40295-013-0007-4.

Picone, J.M., Hedin, A.E., Drob, D.P., Aikin, A.C., 2002. NRLMSISE-00 empirical model of the atmosphere: statistical comparisons and scientific issues. J. Geophys. Res. 107 (A12), 1468. https://doi.org/10.1029/2002JA009430.

Richmond, A.D., 1979. Thermospheric heating in a magnetic storm: dynamic transport of energy from high to low latitudes. J. Geophys. Res. 84, 5259–5266.

Sutton, E.K., Forbes, J.M., Nerem, R.S., 2005. Global thermospheric neutral density and wind response to the severe 2003 geomagnetic storms from CHAMP accelerometer data. J. Geophys. Res. 110, A09S40. https://doi.org/10.1029/2004JA010985.